Original Article

Correlation between vertebral bone mineral density and multi-level virtual non-calcium imaging parameters from dual-layer spectral detector computed tomography

Yanhui Yang[1,2], Jing Hou[2], Yue Niu[1,2], Yi Zhang[1,2], Tao Luo[2], Qiang Lu[2], Yi Fu[3], Yu Wang[4], Xiaoping Yu[1,2]

[1]Department of Diagnostic Radiology, Graduate Collaborative Training Base of Hunan Cancer Hospital, Hengyang Medical School, University of South China, Hengyang, China; [2]Department of Diagnostic Radiology, Hunan Cancer Hospital and the Affiliated Cancer Hospital of Xiangya School of Medicine, Central South University, Changsha, China; [3]Medical Department, Hunan Cancer Hospital and the Affiliated Cancer Hospital of Xiangya School of Medicine, Central South University, Changsha, China; [4]Clinical and Technical Support, Philips Healthcare, Shanghai, China

Contributions: (I) Conception and design: Y Yang, X Yu; (II) Administrative support: Y Fu, X Yu; (III) Provision of study materials or patients: T Luo, Q Lu, Y Wang, X Yu; (IV) Collection and assembly of data: Y Yang, J Hou, Y Niu, Y Zhang; (V) Data analysis and interpretation: Y Yang, J Hou, X Yu; (VI) Manuscript writing: All authors; (VII) Final approval of manuscript: All authors.

Correspondence to: Xiaoping Yu, MD. Department of Diagnostic Radiology, Graduate Collaborative Training Base of Hunan Cancer Hospital, Hengyang Medical School, University of South China, 28 Changsheng West Road, Zhengxiang District, Hengyang 421001, China; Department of Diagnostic Radiology, Hunan Cancer Hospital and the Affiliated Cancer Hospital of Xiangya School of Medicine, Central South University, 283 Tongzipo Road, Yuelu District, Changsha 410013, China. Email: yuxiaoping@hnca.org.cn.

Background: Virtual non-calcium (VNCa) imaging based on dual-energy computed tomography (CT) plays an increasingly important role in diagnosing spinal diseases. However, the utility of VNCa technology in the measurement of vertebral bone mineral density (BMD) is limited, especially the VNCa CT value at multiple calcium suppression levels and the slope of VNCa curve. This retrospective cross-sectional study aimed to explore the correlation between vertebral BMD and new VNCa parameters from dual-layer spectral detector CT.

Methods: The dual-layer spectral detector CT and quantitative CT (QCT) data of 4 hydroxyapatite (HAP) inserts and 667 vertebrae of 234 patients (132 male and 102 female) who visited a university teaching hospital between April and May 2023 were retrospectively analyzed. The BMD values of 3 vertebrae (T12, L1, and L2) and inserts were measured using QCT, defined as QCT-BMD. The VNCa CT values and the slope λ of the VNCa attenuation curve of vertebrae and inserts were recorded. The correlations between VNCa parameters (VNCa CT value, slope λ) and QCT-BMD were analyzed.

Results: For the vertebrae, the correlation coefficient ranged from −0.904 to 0.712 (all $P<0.05$). As the calcium suppression index (CaSI) increased, the correlation degree exhibited a decrease first and then increased, with the best correlation ($r=-0.904$, $P<0.001$) observed at the index of 25%. In contrast, the correlation coefficient for the inserts remained relatively stable ($r=-0.899$ to −1, all $P<0.05$). For the vertebrae, the values of 3 slopes λ (λ1, λ2, and λ3) derived from the VNCa attenuation curve were 6.50±1.99, 3.75±1.15, and 2.04±0.62, respectively. Regarding the inserts, the λ1, λ2, and λ3 values were 11.56 [interquartile range (IQR): 2.40–22.62], 6.68 (IQR: 1.39–13.49), and 3.63 (IQR: 0.75–7.8), respectively. For the vertebrae, all 3 correlation coefficients between 3 slopes λ and QCT-BMD were 0.956 (all $P<0.05$). For the inserts, the 3 correlation coefficients were 0.996, 0.998, and 1 (all $P<0.05$), respectively.

Conclusions: A promising correlation was detected between VNCa CT parameters and QCT-BMD in vertebrae, warranting further investigation to explore the possibility of VNCa imaging to assess BMD.

Keywords: Bone mineral density (BMD); computed tomography (CT); X-ray; virtual non-calcium imaging (VNCa imaging); dual-layer spectral computed tomography (dual-layer spectral CT)

Submitted Nov 01, 2023. Accepted for publication Mar 16, 2024. Published online Apr 12, 2024.
doi: 10.21037/qims-23-1543
View this article at: https://dx.doi.org/10.21037/qims-23-1543

Introduction

Osteoporosis is a disease involving reduced bone mass and impaired bone quality (1,2). It is one of the most common diseases in an aging society. Osteoporosis and secondary fractures can increase the pain of patients, affect their quality of life, and bring a huge economic burden to society (3,4). Therefore, it is necessary to accurately assess the bone mineral density (BMD) of patients, which helps predict osteoporosis and guide patients to carry out corresponding medical behaviors to benefit patients and society. The metabolic activity of vertebral trabecular bone is much higher than that of cortical bone (5). Therefore, it is more important to pay attention to the changes in trabecular bone density in the process of age growth or disease treatment. Currently, dual-energy X-ray absorptiometry (DXA) is a common and important method for diagnosing osteoporosis (6). However, DXA cannot make a differentiation between cancellous and cortical bones because it is based on a 2-dimensional (2D) image. DXA is also susceptible to false negative results due to spinal deformities and abdominal aortic calcification (7). Recently, quantitative computed tomography (QCT), which employs 3-dimensional (3D) reconstruction, has been shown to provide a more accurate measurement of BMD compared to DXA (8). QCT can also separately measure the BMD of cortical and cancellous bones (9). It is unaffected by vertebral size, shape, degeneration, vascular calcification, and other factors (10). However, QCT requires specialized CT scanning protocol, calibration phantom, and analysis software (11), making it a time-consuming, laborious, and expensive option. Therefore, it is necessary to explore more convenient, economical, and available approaches to aid in the evaluation of vertebral BMD.

Among different kinds of newly developing CT techniques, dual-layer spectral detector CT (DLCT) simultaneously acquires 2 sets of high- and low-energy X-ray data through a special dual-layer detector (12,13). Consequently, it achieves better material separation, noise reduction, and artifact reduction than other kinds of dual-energy CT (DECT) (14). DLCT can also leverage both the dual-energy analysis benefits of DXA and the 3D advantages of QCT in the measurement of BMD (15). Additionally, it allows retrospective analysis of dual-energy data without the need for prospective CT scanning protocol for dual-energy data collection, which is more convenient in clinical practice. Virtual non-calcium (VNCa) imaging is a technique used to adjust the contribution of calcium-containing voxels to the attenuation value of tissues on DECT (16-18). The calcium suppression algorithm used in this process determines the level of calcium removal, and the target level of calcium content is adjusted by an user-defined calcium suppression index (CaSI), which can usually be selected in the range of 25% to 100% (18,19). VNCa imaging has exhibited significant diagnostic value in spinal diseases, such as identifying bone marrow edema in vertebral fractures, differentiating vertebral metastases from bone islands, and detecting spinal cord infiltration in multiple myeloma (19-21). However, there is limited research regarding the correlation between BMD and VNCa imaging parameters [such as regular CT value, CT value of calcium, and fat fraction (FF)] in vertebrae and the humerus (21-23). Thus, this study aimed to investigate the correlation between the VNCa parameters and BMD of vertebrae in DLCT, as well as the potential of using VNCa imaging in the assessment of BMD. We present this article in accordance with the STROBE reporting checklist (available at https://qims.amegroups.com/article/view/10.21037/qims-23-1543/rc).

Methods

Participants

The study was conducted in accordance with the Declaration of Helsinki (as revised in 2013). The study was approved by the Hunan Cancer Hospital of Medicine Ethics Committee. The need for obtaining written informed consent from participants was waived due to the nature of the retrospective analysis. Initially, 275 patients who had available abdominal non-enhanced DLCT and QCT data performed between April and May 2023 were included in this study. All included patients were collected from out- and in-patient clinics of Hunan Cancer Hospital. Patients were excluded if they had bone metastasis, poor DLCT image quality, or incomplete clinical or QCT data (data had not been completely transmitted to the QCT post-processing workstation). This study focused on 3

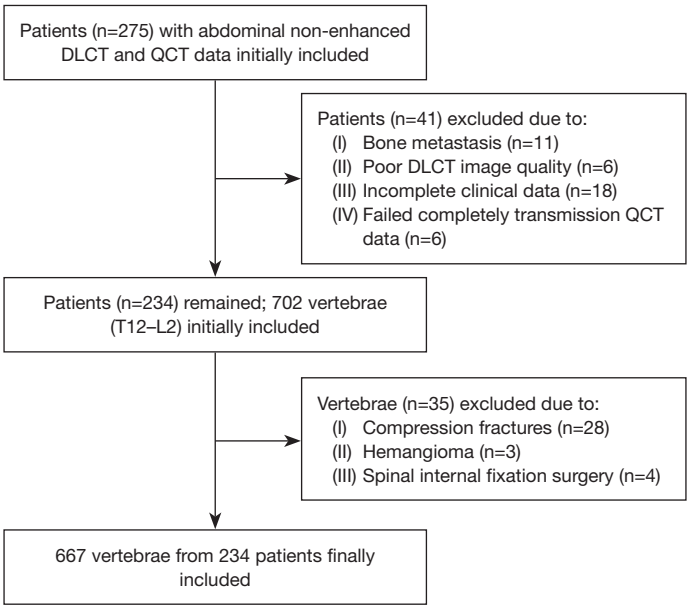

Figure 1 Flow chart illustrating the stepwise inclusion of patients and vertebrae. DLCT, dual-layer spectral detector computed tomography; QCT, quantitative computed tomography.

vertebrae (T12, L1 and L2). A vertebra was excluded if it had compression fractures of grade 2 or higher, hemangioma, or spinal internal fixation surgery. The degree of vertebra compression was evaluated according to Genant's criteria (24). A junior radiologist reviewed the CT images and excluded patients and vertebrae that did not meet the research criteria. When uncertain, the decision was made after consulting with a superior radiologist. The flow chart of inclusion and exclusion is shown in *Figure 1*. Patients' demographic data, including age, gender, height, and body mass index (BMI) were extracted from the hospital's medical record system.

A bone density calibration (BDC) phantom (QRM, Moehrendorf, Germany) containing 6 cylindrical inserts was used to simulate vertebrae with different BMD in this study. The nominal hydroxyapatite (HAP) concentrations of the 6 inserts are 0, 98.8, 201.9, 390.5, 599.1 and 793.7 mg/cm^3, respectively. We defined the HAP concentration as HAP-BMD.

CT data acquirement

All the patients underwent abdominal DLCT scans on a DLCT scanner (IQon Spectral CT; Philips Healthcare, Best, Netherlands) without intravenous administration of contrast agent. The scanning parameters were as follows: tube voltage,120 kVp; adaptive tube current; pitch, 0.5; gantry rotation time, 0.5 s; section collimation 64×0.625 mm; reconstructed slice thickness and interval, 0.992 mm. The BDC phantom was scanned using the same CT scanner and parameters as for the patient. A Model 4 calibration phantom (Mindways Software Inc., Austin, TX, USA) was used for quality assurance calibration before daily scanning of the patients to control the stability of CT scanner. After CT scanning, spectrum-based images and conventional CT images were reconstructed from the raw CT data for subsequent VNCa and QCT analysis.

VNCa imaging analysis

The spectrum-based images were transferred to the post-processing workstation (IntelliSpace Portal, Version 10.0, Philips Healthcare) for VNCa imaging analysis. This post-processing software can automatically generate the axial, coronal and sagittal images of vertebral body, and these images can be simultaneously re-sliced. Multi-level VNCa images were reconstructed with CaSI from 25% to 90%, at intervals of 5%.

For each vertebra (T12, L1, and L2) at each CaSI level, 3 elliptical regions of interest (ROIs) were manually drawn. The ROIs were delineated in the conventional CT image, covering as much of cancellous bone as possible,

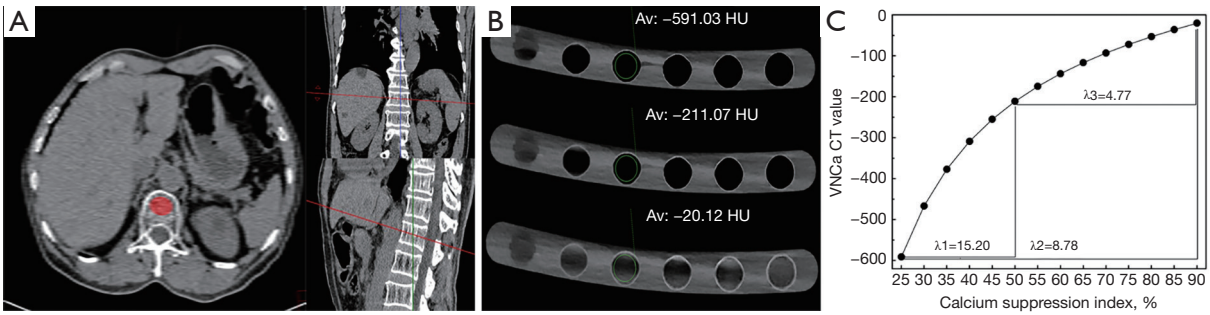

Figure 2 Measurement example of vertebra and insert, and slopes of corresponding insert. (A) The measurement process of L1 in the conventional CT image. (B) The measurement process of an insert (HAP-BMD: 201.9 mg/cm^3) in the VNCa images at CaSI of 25%, 50%, and 90%. (C) The slopes (λ1, λ2, and λ3) values of the VNCa curve of this insert were 15.20, 8.78, and 4.77, respectively. Av, average computed tomography value; HU, Hounsfield unit; VNCa, virtual non-calcium; CT, computed tomography; HAP, hydroxyapatite; BMD, bone mineral density; CaSI, calcium suppression index.

while avoiding the inclusion of cortical bone and posterior vertebral venous plexus (*Figure 2A*). Firstly, an elliptical ROI was placed in the anterior 2/3 at the middle section of the trabecular compartment of the vertebral body on its axial image, and the ROI position was adjusted manually to make it parallel to the upper and lower endplates of vertebrae. Then, using the same method, the delineation of the other 2 ROIs was performed at the adjacent up and down sections of vertebral body. Before delineation, the vertebral images were re-sliced to correct for vertebra cyrtosis if necessary. Since the conventional CT and VNCa images were perfectly aligned in space, the ROIs in the conventional CT image could be automatically applied to the VNCa images at different CaSI levels.

For each vertebra, the VNCa CT value at each CaSI level was the average of the CT values obtained from the 3 ROIs. A circular ROI with a size of approximately 150 mm^2 at the middle level of each insert of the phantom was drawn to obtain its VNCa CT value (*Figure 2B*). Notably, the VNCa CT values of 2 inserts (HAP-BMD: 599.1 and 793.7 mg/cm^3, respectively) were –1,024 Hounsfield units (HU), that is to say, the CT value of air, which indicated reaching the lower limit of CT value measurement and an inaccurate result. In addition, these 2 HAP-BMD values were markedly higher than the ordinary BMD values of human vertebrae. Therefore, these 2 inserts were not included in subsequent analysis.

The slope value was derived from the VNCa attenuation curve of each vertebra and insert, with the formula: λ= (HUCaSI A – HUCaSI B)/[100×(A – B)], where A and B represent 2 different CaSI values, and HU indicates the VNCa CT value at the corresponding CaSI level. Considering the subsequent findings during our data processing that whether in the vertebrae or the phantom, the correlation between the slope and QCT-BMD was the same or very similar, so we selected three representative CaSI values (i.e., 25%, 50%, and 90%) that corresponds to high, middle, and low calcium suppression levels, respectively, and calculated their slopes, as conducted in a previous work (18). We defined λ1=(HU50% – HU25%)/25, λ2=(HU90% – HU25%)/65, and λ3=(HU90% – HU50%)/40.

BMD measurement in QCT

The conventional CT images were transferred to the QCT workstation. We defined the BMD measured by QCT as QCT-BMD. The QCT-BMD values of T12, L1, and L2 vertebrae were derived using spine measurement module of the 3D spine function version 6.10 of Mindways QCT pro software (Mindways Software Inc., USA). The volume of interest (VOI) with a fixed height of 9 mm was semi-automatically placed at the middle level of the vertebrae. The in-plane dimensions of the VOI were adjusted according to the condition of the vertebrae to cover as much of cancellous bone as possible, while avoiding the inclusion of cortical bone and posterior vertebral venous plexus (*Figure 3*). Each insert in the phantom was regarded as individual vertebra, and its QCT-BMD was measured using the same method as vertebra.

Statistical analysis

All measurements process of VNCa CT values and QCT-BMD were conducted by a radiologist with 12 years of

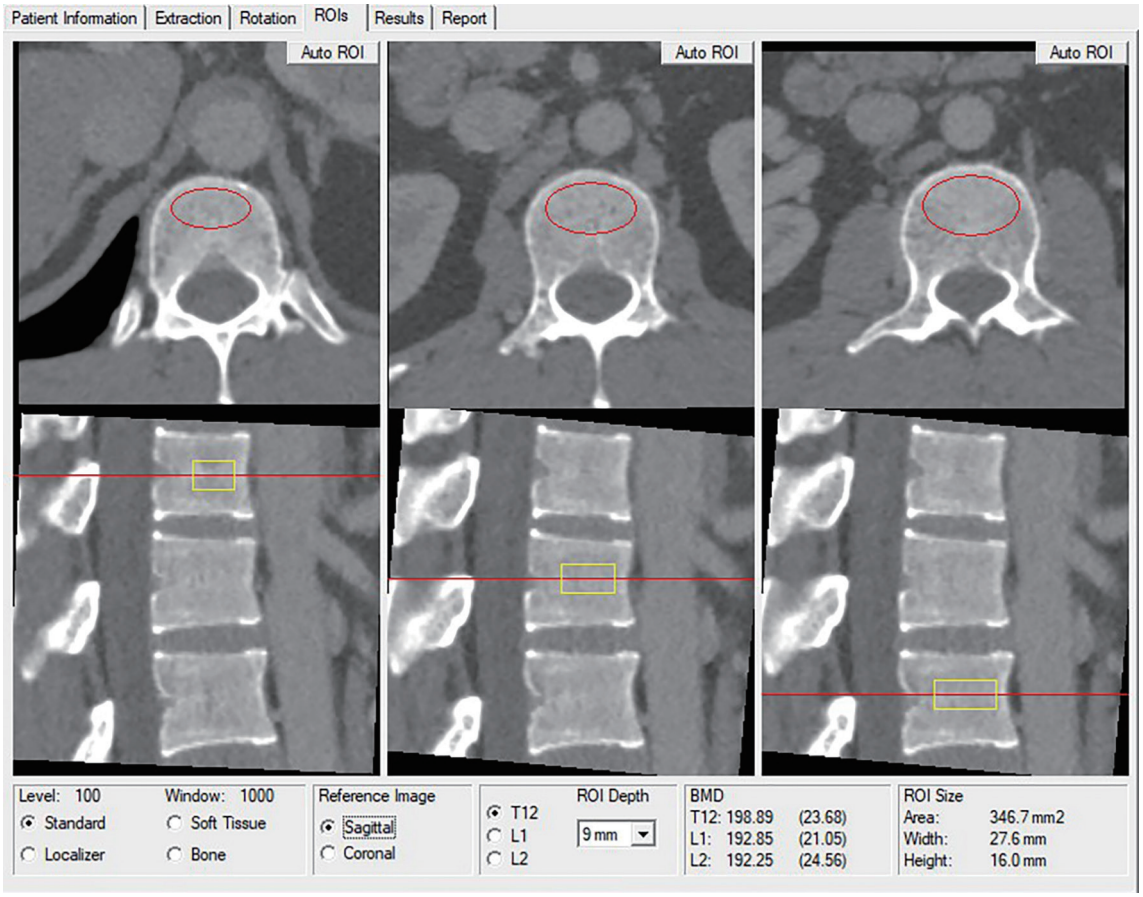

Figure 3 Schematic diagram of vertebral BMD measured using QCT software. The red oval area in the axial section and the yellow rectangle in the sagittal plane are the cross-sectional area and the sagittal plane area of VOI, respectively. The red line in the sagittal plane presents the central level of VOI. VOI, volume of interest; ROI, region of interest; BMD, bone mineral density; QCT, quantitative computed tomography.

experience in the diagnosis of musculoskeletal disease. Statistical analysis was conducted using dedicated commercial software (SPSS 26.0, Armonk, NY, USA). The Kolmogorov-Smirnov or Shapiro-Wilk test was used to assess the normality of continuous variables. Continuous variables with normal distribution were expressed as mean ± standard deviation (SD), and continuous variables with non-normal distribution were expressed as median [interquartile range (IQR)]. Pearson or Spearman correlation analysis was employed to evaluate the correlations of the VNCa CT values, slope λ, and HAP-BMD with QCT-BMD, respectively. Rank sum test was conducted to compare the difference in the absolute values of correlation coefficient (namely correlation degree) between vertebrae and inserts. A P value <0.05 was considered statistically significant.

Results

Correlation between HAP-BMD and QCT-BMD of phantom

The QCT-BMD for the 4 inserts were 0.9, 126.2, 242.3, and 460.3 mg/cm^3, respectively, which were higher than HAP-BMD values (0, 98.8, 201.9, and 390.5 mg/cm^3, respectively). There was an excellent correlation (r=1, P<0.001) between QCT-BMD and HAP-BMD of inserts.

VNCa CT values of vertebrae and phantom

This study finally included 667 vertebrae from 234 patients (132 male and 102 female). The patients' mean age, body weight, and BMI was 57.1±12.0 years (range, 21–86 years),

Table 1 The VNCa CT values of the vertebrae and inserts at different calcium suppression index

CaSI	Vertebrae (n=667)	Inserts (n=4)	Insert (0 mg/cm^3)	Insert (98.8 mg/cm^3)	Insert (201.9 mg/cm^3)	Insert (390.5 mg/cm^3)
25%	−209.3 (−264.5 to −172.4)	−480.6±415.9	−24.8	−307.2	−591.0	−999.3
30%	−158.6 (−198.4 to −132.1)	−382.3±326.5	−20.3	−242.4	−466.7	−842.5
35%	−122.4 (−151.3 to −102.2)	−307.4±262.4	−17.0	−195.6	−376.9	−677.2
40%	−95.0 (−116.4 to −79.9)	−250±213.7	−14.5	−160.0	−308.7	−551.7
45%	−73.1 (−88.6 to −60.9)	−205.7±175.3	−12.5	−132.0	−254.9	−452.7
50%	−57.0±19.3	−169.2±144.0	−10.9	−109.2	−211.1	−372.1
55%	−41.3±16.5	−138.7±118.0	−9.6	−90.1	−174.6	−304.9
60%	−27.8 (−34.2 to −21.3)	−112.8±95.7	−8.5	−73.9	−143.5	−247.8
65%	−16.1 (−23.1 to −10.3)	−90.4±76.6	−7.5	−59.9	−116.6	−198.3
70%	−6.6±14.8	−70.7±60.0	−6.7	−47.6	−93.0	−154.9
75%	2.5±15.6	−53.2±44.8	−5.9	−36.7	−72.0	−116.2
80%	10.7 (2.8 to 19.6)	−37.5±31.3	−5.2	−26.8	−53.1	−81.4
85%	18.0±17.9	−23.1±19.1	−4.5	−17.8	−35.9	−49.7
90%	24.8±19.1	−10.0±8.2	−4.0	−9.6	−20.1	−20.6

Data are presented as mean ± standard deviation, median (interquartile range) or number. VNCa, virtual non-calcium; CT, computed tomography; CaSI, calcium suppression index.

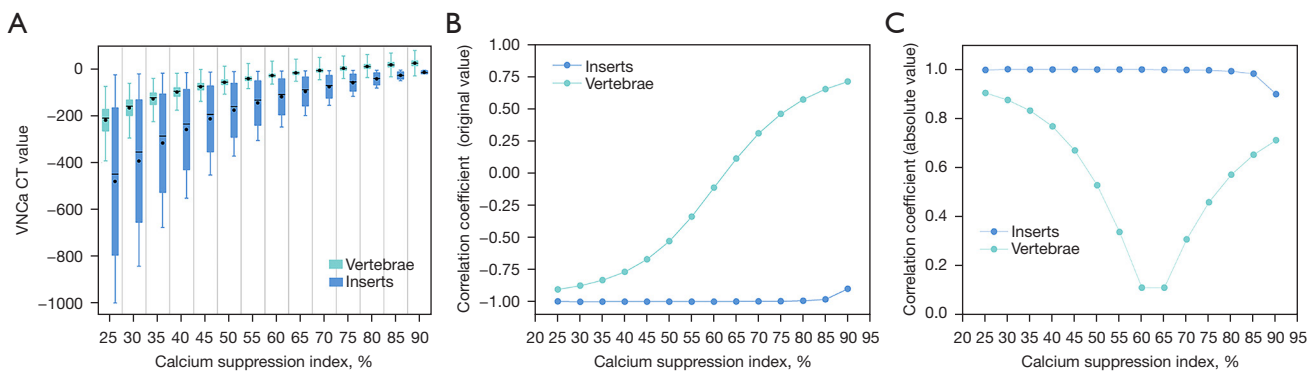

Figure 4 Box plot of VNCa CT values and line chart between VNCa CT values and QCT-BMD of the vertebrae and the inserts at different calcium suppression levels. (A) Box plot of VNCa CT values; (B) line chart of the original values of correlation coefficient between VNCa CT values and QCT-BMD; (C) line chart of the absolute values of correlation coefficient between VNCa CT values and QCT-BMD. VNCa, virtual non-calcium; CT, computed tomography; QCT, quantitative computed tomography; BMD, bone mineral density.

60.62±10.97 kg (range, 35–98 kg), and 22.90±3.63 kg/m^2 (range, 14.02–36.00 kg/m^2), respectively. The VNCa CT values of vertebrae and phantom at each CaSI are shown in *Table 1*. The VNCa CT values of both vertebrae and phantom increased with the increase of CaSI value. However, with the increase of CaSI value, the increase rate of VNCa CT value slowed down (*Figure 4A*).

Correlations between QCT-BMD and VNCa imaging parameters (slope and CT value)

The mean QCT-BMD value of the 667 vertebrae was 120.9±41.0 mg/cm^3 (range, 24.1–231.6 mg/cm^3). *Figure 4B* shows the original values of correlation coefficient between QCT-BMD and VNCa CT values of the vertebrae and

Table 2 The representative slope values (λ1, λ2, and λ3) of the vertebrae and inserts

Slope	Vertebrae (n=667)	Inserts (n=4)	Insert (0 mg/cm^3)	Insert (98.8 mg/cm^3)	Insert (201.9 mg/cm^3)	Insert (390.5 mg/cm^3)
λ1	6.50±1.99	11.56 (2.40–22.62)	0.55	7.92	15.2	25.09
λ2	3.75±1.15	6.68 (1.39–13.49)	0.32	4.58	8.78	15.06
λ3	2.04±0.62	3.63 (0.75–7.8)	0.17	2.49	4.77	8.79

Data are presented as mean ± standard deviation, median (interquartile range) or number. λ1, λ2, and λ3 correspond to the slope of VNCa attenuation curve at CaSI from 25% to 50%, from 25% to 90%, and from 50% to 90%, respectively. VNCa, virtual non-calcium; CaSI, calcium suppression index.

phantom at different CaSI levels. For the vertebrae, the original values of correlation coefficient ranged from –0.904 to 0.712 (all P<0.05), with an average of –0.158±0.617, and the average of the absolute values of correlation coefficient was 0.561±0.263. As CaSI increased, the absolute values of correlation coefficient was shown to decrease first and then increase, with the best correlation degree (r=0.904, P<0.001) observed at the CaSI of 25% (*Figure 4C*). In contrast, for the phantom, the correlation coefficient remained relatively stable (r=–0.899 to –1, all P<0.05), with an average of –0.990±0.027 (*Figure 4B*). Rank sum test showed that the absolute values of correlation coefficients between VNCa CT and QCT-BMD were significantly higher for the phantom than for the vertebrae (Z=–4.48, P<0.001). The correlation coefficient between vertebral QCT-BMD and conventional HU was 0.980 (P<0.001). For the vertebrae, the correlation coefficients between VNCa CT value and conventional HU at different CaSI were between –0.932 and 0.875, and the absolute value of correlation coefficients ranged from 0.121 to 0.932. The maximum correlation coefficient of 0.932 was observed at the CaSI of 25%, whereas the minimum of 0.121 was found when the CaSI was 60%.

The values of 3 slopes λ (λ_1, λ_2, and λ_3) derived from the VNCa attenuation curve for the vertebrae and inserts are shown in *Table 2*. The scatter plot and linear regression equation of the VNCa parameters (VNCa CT value and slope) versus QCT-BMD of the vertebrae are shown in *Figure 5*. The statistical results of linear regression equation between slopes and QCT-BMD are shown in Supplementary Result S1 (Appendix 1). The scatter plot, linear regression equation, and its statistical results of the VNCa slopes and HAP-BMD of the phantom are shown in Figure S1. For the vertebrae, all the 3 correlation coefficients between three slopes λ and QCT-BMD were 0.956 (all P<0.001). For the phantom, the corresponding 3 correlation coefficients were 0.996, 0.998, and 1 (all P<0.05), respectively. *Figure 6* shows example of the VNCa CT images and corresponding parameters at representative CaSI levels for L1 vertebra in 2 patients with low and high QCT-BMD, respectively.

Discussion

This study focused the correlation between vertebral BMD and multi-level VNCa parameters from DLCT, and demonstrated good correlation between QCT-BMD and VNCa CT values, as well as between QCT-BMD and slopes of VNCa curve. Our attempt to utilize VNCa parameters may provide clues for the development of a potential proxy measurement of vertebral BMD without the need for QCT.

VNCa reconstruction is capable of producing with different degree of calcium suppression. CaSI is an index that reflects the degree of removal of calcium component on the VNCa image, resulting in the virtual HU resembling the expected HU obtained without the corresponding contribution of calcium to CT attenuation (19). By manually adjusting the CaSI value, the contribution of calcium-containing voxels to the VNCa CT value can be completely or partially removed. Usually, CaSI value can be selected from 25% to 100% (19) . Theoretically, a low CaSI value indicates a high degree of calcium suppression, a low contribution of calcium, and subsequently a small VNCa CT number, whereas a high CaSI value represents a low degree of calcium suppression, a high contribution of calcium, and therefore a large CT number. This theory can explain our observation that the VNCa CT values of both vertebra and phantom increased with the increase of CaSI value.

In regard to the correlation between QCT-BMD and VNCa CT values for the vertebra, a maximum (r=–0.904) was found at the CaSI of 25%, indicting a good correlation. Our finding was similar to a prior study that the VNCa

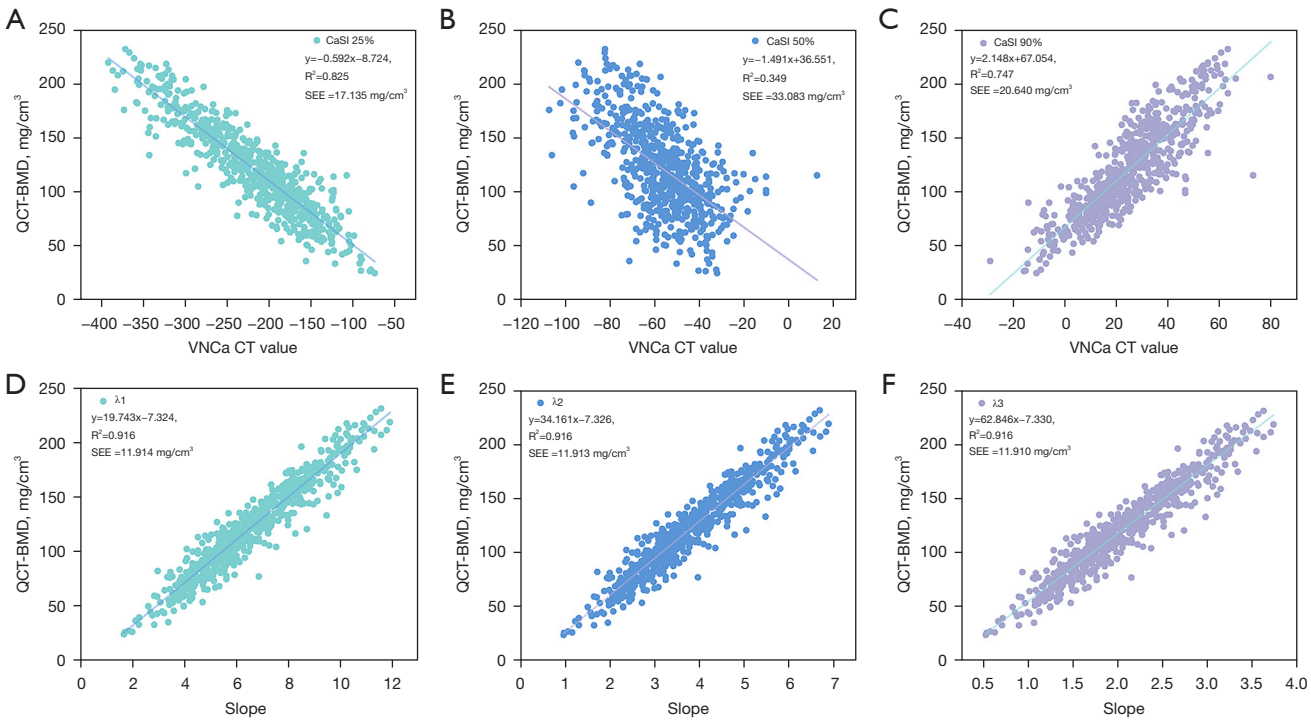

Figure 5 The scatter plot and linear regression equation of the VNCa parameters (VNCa CT value and slope) *vs*. QCT-BMD of the vertebrae. The scatter plot and linear regression equation between QCT-BMD with VNCa parameters of (A) CaSI 25%, (B) CaSI 50%, (C) CaSI 90%, (D) λ1, (E) λ2, and (F) λ3. QCT, quantitative computed tomography; BMD, bone mineral density; VNCa, virtual non-calcium; CT, computed tomography; CaSI, calcium suppression index; SEE, standard error of estimate.

Figure 6 Example of the VNCa CT images and VNCa curves at representative calcium suppression levels in 2 patients at L1 vertebra with different levels of QCT-BMD. Each column from left to right represents the VNCa CT images at the calcium suppression index of 25%, 50%, and 90%, respectively. (A) Patient A with low (70.8 mg/cm^3) QCT-BMD. The slopes λ1, λ2, and λ3 values of the VNCa curve were 3.67, 2.21, and 1.12, respectively. (B) Patient B with high (160.5 mg/cm^3) QCT-BMD. The slopes λ1, λ2, and λ3 values of the VNCa curve were 8.07, 4.86, and 2.46, respectively. Av, average computed tomography value; HU, Hounsfield unit; VNCa, virtual non-calcium; CT, computed tomography; QCT, quantitative computed tomography; BMD, bone mineral density.

values of humerus correlated significantly (R^2=0.653; P<0.001) with the CT value of calcium (CaCT), an indicator of the calcium concentration (22). However, these correlations in the present study varied obviously with the CaSI value, suggesting attention should be paid to the level of calcium suppression when discussing correlation between QCT-BMD and VNCa CT values for the vertebra.

Interestingly, we also found that as the CaSI increased, the absolute values of the correlation coefficient exhibited a decrease followed by an increase. In our opinion, this change might be related to the algorithms used in VNCa imaging. In VNCa images, different CT values are assigned to the calcium component according to different CaSI values, whereas the CT values of the non-calcium component remain unchanged from conventional CT. As the CaSI value increases, the assigned CT value (i.e., VNCa CT number) for calcium also increases. According to our initial observations on the cortical bone of the femur shaft which is composed almost entirely of calcium, the assigned CT value for calcium in our study ranged from −1,024 HU at CaSI of 25% to approximate 200 HU at CaSI of 90%.

When the CaSI is very high (e.g., 90%), the CT value of calcium is much higher than that of the non-calcium component, which will result in a significant difference in the CT values between the calcium and non-calcium components. Under this circumstance, the CT value of the vertebra is remarkably influenced by the calcium component, far more than by the non-calcium component. Thus, the correlation of the vertebral CT value to the calcium component is much higher than to the non-calcium component. As the amount of calcium directly determines BMD, thus the correlation of the vertebra CT value to BMD is markedly better at higher CaSI values. When the CaSI is very low (e.g., 25%), the CT value of calcium is much lower than that of the non-calcium component, and therefore it will also result in a significant difference in the CT values between the calcium and non-calcium components. Similarly, the correlation of the vertebra CT value to BMD is also very good at low CaSI values. When CaSI is at an intermediate value (e.g., 60%), the CT value of calcium is relatively close to that of the non-calcium component, which will result in a very small difference in the CT values between the calcium and non-calcium components. At this point, the change in the calcium component within the vertebra has a relatively small impact on the change of the vertebral CT value, resulting in a weaker correlation between the vertebral CT value and BMD.

In VNCa images, the contribution of calcium to VNCa CT value will decrease with the decrease of CaSI value. Considering that the contribution of non-calcium components to the CT value of cancellous bone is not affected by CaSI, therefore, the lower the CaSI value, the more obvious the CT value is affected by non-calcium components, whereas the influence of calcium is less pronounced. That is to say, under the circumstance of lower CaSI value, once the non-calcium components change, the CT value of cancellous bone will be more likely to undergo sensitive changes accordingly. Thus, in our opinion, a lower CaSI value may be more helpful in characterizing the non-calcium components of cancellous bone. According to our observations, when the CaSI is 25%, the contribution of calcium to the VNCa CT values will be almost fully removed. In this circumstance, the CT value of cancellous bone is almost entirely determined by non-calcium components, and is unaffected by calcium. Therefore, we speculate that 25% might be the best CaSI level to characterize the non-calcium components of cancellous bone by using VNCa image.

In this study, the correlation degree between VNCa CT values and QCT-BMD was higher for the inserts than it was for vertebrae. The difference in the inner compositions between vertebrae and inserts may provide a possible interpretation for the above findings in our study. The BDC phantom is a simple analog that simulates the human spine using HAP, water, and fat, which homogeneously distribute in the insert. Different from inserts, human vertebrae contain a greater variety and more complex components besides calcium, water, and fat, which distribute heterogeneously in cancellous bone.

As for the relationship between VNCa CT value and QCT-BMD, the variation in the correlation coefficients among different CaSI levels was significantly larger for the vertebrae than for the phantom in the present study. In our opinion, this could also be related to the notable differences in the variety and complexities of internal components between vertebrae and inserts. Firstly, the calcium components might contribute differently to the VNCa CT values at different calcium suppression levels, resulting in a disproportionate relationship between the variations on VNCa CT value and changes in CaSI value. Secondly, QCT-BMD may not accurately reflect the true calcium content of the vertebrae, it may be influenced by complicated components of the vertebrae, such as fat. For instance, the existence of bone marrow adipose tissue leads to an underestimation of spine BMD, and this error will amplify with higher fat content (25). A similar finding

was also reported in another DECT study in which the utilization of substance decomposition method (fat *vs.* HAP) for diagnosing osteoporosis yielded unsatisfactory results, with an AUC of only 0.594 (26).

The slope of VNCa curve reflects the change in the CT values between 2 different CaSI levels. A larger slope value represents a more obvious change of VNCa CT value when CaSI level varies, which indicates that the VNCa curve is steeper. According to the principle of VNCa imaging, the slope is related to calcium, and is irrelevant to non-calcium substance (such as bone marrow), because the VNCa CT value of non-calcium substance is constant at different CaSI levels. Considering that the VNCa CT value was significantly correlated with QCT-BMD due to their common relation with calcium and that the slope was directly derived from VNCa CT value, the slope should theoretically correlate with BMD. In the present study, we selected 3 representative CaSI at high, middle, and low levels of calcium suppression to explore the relation between slope and BMD. Good correlation was revealed between QCT-BMD and slopes of VNCa curve, which supports the potential relationship between slope and actual BMD in the human vertebra body. Moreover, we calculated the slopes of the inserts with explicit nominal HAP concentrations based on gold-standard chemical measurement, and found that a larger HAP concentration (i.e., larger BMD) was associated with larger slopes, which further strengthens the relationship between slope and BMD.

In this study, we used a standard phantom to verify the correlation between BMD measured by QCT and nominal BMD (i.e., HAP concentrations). Excellent correlation was found between the QCT-BMD and HAP-BMD values of the internal inserts in this study, which further verified previous investigations on the reliability of QCT in the measurement of BMD (27,28). A prior study also verified the accuracy of QCT in measuring BMD based on the European spine phantom (ESP) (29,30). Of note, both our and previous studies on phantom found that the BMD value measured by QCT was usually higher than the HAP concentrations value (28). A possible reason for this interesting phenomenon is that the non-calcium components might have negative influence on the measurement of BMD. For example, high bone marrow FF is a source of error in the measurement of BMD using QCT (31).

Similar to our study, a few recent works have also focused on the potential utility of VNCa imaging in the measurement of BMD. The vertebral CT value of calcium (CM), calcium density (CaD), and FF derived from dual-source CT data exhibited significantly associations with QCT-BMD in a previous investigation on VNCa imaging (23). In regard to the diagnosis of vertebral osteoporosis, the regressive BMD value generated from a multiple linear regression equation, which included CM, CaD, and FF, demonstrated a sensitivity of 90.0% and a specificity of 92.0% (23). Yu *et al.* (22) also found that VNCa value was a significant predictor of the calcium concentration in the humerus. These encouraging findings may enhance the possibility to directly measure BMD using the DLCT data collected in routine clinical work, thereby potentially eliminating the need for QCT and DXA in the future. As we know, QCT is not easily available in clinical practice because it requires specialized CT scanning protocol, calibration phantom, and processing software. When measuring bone density, if DXA data is additionally collected instead of directly utilizing existing DLCT data, it may result in increased radiation exposure and medical costs. Moreover, compared to the other types of DECT, DLCT does not require the prospective selection of dual-energy scanning protocol, which simplifies the operation procedure and increases the effectiveness of beam hardening correction (32,33).

This study has some limitations. Firstly, its retrospective nature may have introduced selection bias. Secondly, the QCT-BMD of vertebrae may not accurately represent the actual BMD. However, obtaining an accurate quantification of BMD requires the use of chemical measurement methods, which is scarcely possible to be performed *in vivo*. Thirdly, the phantom used in the study had limited levels of HAP concentrations as the available phantoms are very limited. Nevertheless, the main focus of our study was on human vertebrae rather than on the phantom. Fourth, this study only analyzed T12–L2 vertebrae, and therefore our finding may not be suitable for other vertebrae and extraspinal bones. Finally, although the measurement positions were placed at the middle level of the vertebral body to maintain consistency as far as possible, the location and size of vertebral area for QCT-BMD and VNCa analyses were not accurately matched, which may cause a negative effect on the results of the study.

Conclusions

New VNCa parameters (slope and CT value) at multiple CaSI levels were calculated in human vertebrae *in vivo*, and there existed promising correlations between VNCa CT

parameters and BMD in vertebrae that warrants further investigation to explore the possibility of VNCa imaging to assess BMD.

Acknowledgments

We would like to thank Professor Kun Zhang from the Department of Radiology, First Affiliated Hospital of Hunan University of Chinese Medicine, Changsha, China, for providing us with the BDC phantom.
Funding: None.

Footnote

Reporting Checklist: The authors have completed the STROBE reporting checklist. Available at https://qims.amegroups.com/article/view/10.21037/qims-23-1543/rc

Conflicts of Interest: All authors have completed the ICMJE uniform disclosure form (available at https://qims.amegroups.com/article/view/10.21037/qims-23-1543/coif). Y.W. reports full-time employee of Philips Healthcare from 2022, during the conduct of the study. The other authors have no conflicts of interest to declare.

Ethical Statement: The authors are accountable for all aspects of the work in ensuring that questions related to the accuracy or integrity of any part of the work are appropriately investigated and resolved. The study was conducted in accordance with the Declaration of Helsinki (as revised in 2013). The study was approved by the Hunan Cancer Hospital of Medicine Ethics Committee. The need for obtaining written informed consent from participants was waived due to the nature of the retrospective analysis.

References

1. Osteoporosis prevention, diagnosis, and therapy. JAMA 2001;285:785-95.
2. Consensus development conference: prophylaxis and treatment of osteoporosis. Osteoporos Int 1991;1:114-7.
3. Häussler B, Gothe H, Göl D, Glaeske G, Pientka L, Felsenberg D. Epidemiology, treatment and costs of osteoporosis in Germany--the BoneEVA Study. Osteoporos Int 2007;18:77-84.
4. Moayyeri A, Warden J, Han S, Suh HS, Pinedo-Villanueva R, Harvey NC, Curtis JR, Silverman S, Multani JK, Yeh EJ. Estimating the economic burden of osteoporotic fractures in a multinational study: a real-world data perspective. Osteoporos Int 2023;34:2121-32.
5. Engelke K, Adams JE, Armbrecht G, Augat P, Bogado CE, Bouxsein ML, Felsenberg D, Ito M, Prevrhal S, Hans DB, Lewiecki EM. Clinical use of quantitative computed tomography and peripheral quantitative computed tomography in the management of osteoporosis in adults: the 2007 ISCD Official Positions. J Clin Densitom 2008;11:123-62.
6. Cheng X, Yuan H, Cheng J, Weng X, Xu H, Gao J, Huang M, Wáng YXJ, Wu Y, Xu W, Liu L, Liu H, Huang C, Jin Z, Tian W; Bone and Joint Group of Chinese Society of Radiology, Chinese Medical Association (CMA), Musculoskeletal Radiology Society of Chinese Medical Doctors Association, Osteoporosis Group of Chinese Orthopedic Association, Bone Density Group of Chinese Society of Imaging Technology, CMA*. Chinese expert consensus on the diagnosis of osteoporosis by imaging and bone mineral density. Quant Imaging Med Surg 2020;10:2066-77.
7. Jain RK, Vokes T. Dual-energy X-ray Absorptiometry. J Clin Densitom 2017;20:291-303.
8. Link TM. Osteoporosis imaging: state of the art and advanced imaging. Radiology 2012;263:3-17.
9. Carnevale A, Pellegrino F, Bravi B, Gamberini MR, Gagliardi I, Reverberi R, Zatelli MC, Giganti M, Ambrosio MR. The role of opportunistic quantitative computed tomography in the evaluation of bone disease and risk of fracture in thalassemia major. Eur J Haematol 2022;109:648-55.
10. Löffler MT, Jacob A, Valentinitsch A, Rienmüller A, Zimmer C, Ryang YM, Baum T, Kirschke JS. Improved prediction of incident vertebral fractures using opportunistic QCT compared to DXA. Eur Radiol 2019;29:4980-9.
11. Bredella MA, Daley SM, Kalra MK, Brown JK, Miller KK, Torriani M. Marrow Adipose Tissue Quantification of the Lumbar Spine by Using Dual-Energy CT and

Single-Voxel (1)H MR Spectroscopy: A Feasibility Study. Radiology 2015;277:230-5.
12. Parakh A, Lennartz S, An C, Rajiah P, Yeh BM, Simeone FJ, Sahani DV, Kambadakone AR. Dual-Energy CT Images: Pearls and Pitfalls. Radiographics 2021;41:98-119.
13. Greffier J, Villani N, Defez D, Dabli D, Si-Mohamed S. Spectral CT imaging: Technical principles of dual-energy CT and multi-energy photon-counting CT. Diagn Interv Imaging 2023;104:167-77.
14. Lennartz S, Hokamp NG, Kambadakone A. Dual-Energy CT of the Abdomen: Radiology In Training. Radiology 2022;305:19-27.
15. Van Hedent S, Su KH, Jordan DW, Eck B, Liang F, Kessner R, Kuo JW, Buls N, Klahr P, Ros P, Muzic RF Jr. Improving Bone Mineral Density Assessment Using Spectral Detector CT. J Clin Densitom 2019;22:374-81.
16. Wu H, Zhang G, Shi L, Li X, Chen M, Huang X, Cao X, Tan S, Cui Y, Liang C. Axial Spondyloarthritis: Dual-Energy Virtual Noncalcium CT in the Detection of Bone Marrow Edema in the Sacroiliac Joints. Radiology 2019;290:157-64.
17. Kim JE, Yoo HJ, Chae HD, Choi JY, Hong SH, Kang JH, Yeoh H. Dual-Layer Detector CT With Virtual Noncalcium Imaging: Diagnostic Performance in Patients With Suspected Wrist Fractures. AJR Am J Roentgenol 2021;216:1003-13.
18. Abdullayev N, Große Hokamp N, Lennartz S, Holz JA, Romman Z, Pahn G, Neuhaus V, Maintz D, Krug B, Borggrefe J. Improvements of diagnostic accuracy and visualization of vertebral metastasis using multi-level virtual non-calcium reconstructions from dual-layer spectral detector computed tomography. Eur Radiol 2019;29:5941-9.
19. Neuhaus V, Lennartz S, Abdullayev N, Große Hokamp N, Shapira N, Kafri G, Holz JA, Krug B, Hellmich M, Maintz D, Borggrefe J. Bone marrow edema in traumatic vertebral compression fractures: Diagnostic accuracy of dual-layer detector CT using calcium suppressed images. Eur J Radiol 2018;105:216-20.
20. Fervers P, Fervers F, Kottlors J, Lohneis P, Pollman-Schweckhorst P, Zaytoun H, Rinneburger M, Maintz D, Große Hokamp N. Feasibility of artificial intelligence-supported assessment of bone marrow infiltration using dual-energy computed tomography in patients with evidence of monoclonal protein - a retrospective observational study. Eur Radiol 2022;32:2901-11.
21. Luo H, Zou L, Yang Q, Yuan C, Ma K, Yang S, Luo D, Liu C, Liu Z. Spectral CT assists differentiation of osteoblastic bone metastasis from bone island in newly diagnosed cancer patients. Eur Radiol 2024;34:60-8.
22. Yu Q, Yang J, Zhou C, Xu Z, Liu C, Luo Q, Zhang L. Quantification of bone quality and distribution of the proximal humerus with dual-energy computed tomography. Quant Imaging Med Surg 2023;13:5676-87.
23. Liu Z, Zhang Y, Liu Z, Kong J, Huang D, Zhang X, Jiang Y. Dual-Energy Computed Tomography Virtual Noncalcium Technique in Diagnosing Osteoporosis: Correlation With Quantitative Computed Tomography. J Comput Assist Tomogr 2021;45:452-7.
24. Genant HK, Wu CY, van Kuijk C, Nevitt MC. Vertebral fracture assessment using a semiquantitative technique. J Bone Miner Res 1993;8:1137-48.
25. Laval-Jeantet AM, Roger B, Bouysee S, Bergot C, Mazess RB. Influence of vertebral fat content on quantitative CT density. Radiology 1986;159:463-6.
26. Wang X, Li B, Tong X, Fan Y, Wang S, Liu Y, Fang X, Liu L. Diagnostic Accuracy of Dual-Energy CT Material Decomposition Technique for Assessing Bone Status Compared with Quantitative Computed Tomography. Diagnostics (Basel) 2023;13:1751.
27. Qadan L, Ahmed A. Addressing gaps in osteoporosis screening in kuwait using opportunistic quantitative computer tomography (QCT): a retrospective study. Arch Osteoporos 2023;18:50.
28. Wang L, Su Y, Wang Q, Duanmu Y, Yang M, Yi C, Cheng X. Validation of asynchronous quantitative bone densitometry of the spine: Accuracy, short-term reproducibility, and a comparison with conventional quantitative computed tomography. Sci Rep 2017;7:6284.
29. Roski F, Hammel J, Mei K, Baum T, Kirschke JS, Laugerette A, Kopp FK, Bodden J, Pfeiffer D, Pfeiffer F, Rummeny EJ, Noël PB, Gersing AS, Schwaiger BJ. Bone mineral density measurements derived from dual-layer spectral CT enable opportunistic screening for osteoporosis. Eur Radiol 2019;29:6355-63.
30. Wang M, Wu Y, Zhou Y, Dong J, Hou P, Gao J. The new fast kilovoltage-switching dual-energy computed tomography for measuring bone mineral density. Quant Imaging Med Surg 2023;13:801-11.
31. Cheng X, Li K, Zhang Y, Wang L, Xu L, Liu Y, Duanmu Y, Chen D, Tian W, Blake GM. The accurate relationship between spine bone density and bone marrow in humans. Bone 2020;134:115312.
32. Gassert FT, Hammel J, Hofmann FC, Neumann J, von Schacky CE, Gassert FG, Pfeiffer D, Pfeiffer F, Makowski MR, Woertler K, Gersing AS, Schwaiger BJ. Detection of

Bone Marrow Edema in Patients with Osteoid Osteoma Using Three-Material Decomposition with Dual-Layer Spectral CT. Diagnostics (Basel) 2021;11:953.
33. Mei K, Schwaiger BJ, Kopp FK, Ehn S, Gersing AS, Kirschke JS, Muenzel D, Fingerle AA, Rummeny EJ, Pfeiffer F, Baum T, Noël PB. Bone mineral density measurements in vertebral specimens and phantoms using dual-layer spectral computed tomography. Sci Rep 2017;7:17519.

Cite this article as: Yang Y, Hou J, Niu Y, Zhang Y, Luo T, Lu Q, Fu Y, Wang Y, Yu X. Correlation between vertebral bone mineral density and multi-level virtual non-calcium imaging parameters from dual-layer spectral detector computed tomography. Quant Imaging Med Surg 2024;14(6):3803-3815. doi: 10.21037/qims-23-1543

Supplementary

Appendix 1

Supplementary result S1

The SPSS software results of R^2 and SEE of the linear regression between the VNCa slopes and QCT-BMD of the vertebrae. SEE, standard error of estimate; VNCa, virtual non-calcium; QCT, quantitative computed tomography; BMD, bone mineral density.

1. The results of linear regression between λ1 and QCT-BMD

Variables Entered/Removed

Model	Variables Entered	Variables Removed	Method
1	λ1	.	Enter

Model Summary

Model	R	R Square	Adjusted R Square	Std. Error of the Estimate
1	0.957	0.916	0.916	11.91368

ANOVA

Model		Sum of Squares	df	Mean Square	F	Sig.
1	Regression	1024513.767	1	1024513.767	7218.156	0.000
	Residual	94245.275	665	141.936		
	Total	1118759.042	666			

Coefficients

Model		Unstandardized Coefficients		Standardized Coefficients	t	Sig.
		B	Std. Error	Beta		
1	(Constant)	–7.324	1.578		–4.642	.000
	λ1	19.743	0.232	0.957	84.960	.000

https://dx.doi.org/10.21037/qims-23-1543

2. The results of linear regression between λ2 and QCT-BMD

Variables Entered/Removed			
Model	Variables Entered	Variables Removed	Method
1	λ2	.	Enter

Model Summary				
Model	R	R Square	Adjusted R Square	Std. Error of the Estimate
1	0.957	0.916	0.916	11.91257

ANOVA						
Model		Sum of Squares	df	Mean Square	F	Sig.
1	Regression	1024531.174	1	1024531.174	7219.613	0.000
	Residual	94227.868	665	141.909		
	Total	1118759.042	666			

Coefficients						
Model		Unstandardized Coefficients		Standardized Coefficients	t	Sig.
		B	Std. Error	Beta		
1	(Constant)	−7.326	1.578		−4.643	0.000
	λ2	34.161	0.402	0.957	84.968	0.000

3. The results of linear regression between λ3 and QCT-BMD

Variables Entered/Removed			
Model	Variables Entered	Variables Removed	Method
1	λ3	.	Enter

Model Summary				
Model	R	R Square	Adjusted R Square	Std. Error of the Estimate
1	0.957	0.916	0.916	11.91042

ANOVA						
Model		Sum of Squares	df	Mean Square	F	Sig.
1	Regression	1024565.268	1	1024565.268	7222.466	0.000
	Residual	94193.774	665	141.858		
	Total	1118759.042	666			

Coefficients						
Model		Unstandardized Coefficients		Standardized Coefficients	t	Sig.
		B	Std. Error	Beta		
1	(Constant)	−7.330	1.577		−4.647	.000
	λ3	62.846	0.739	0.957	84.985	.000

https://dx.doi.org/10.21037/qims-23-1543

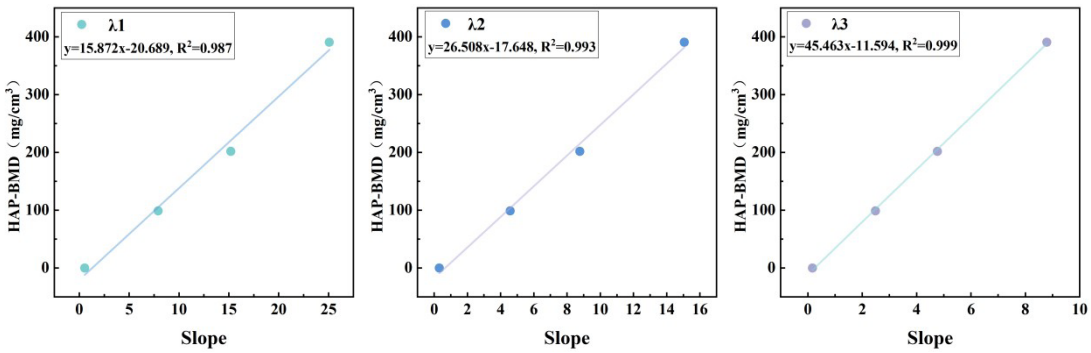

Figure S1 Scatter plots and linear regression equations of slopes (λ1, λ2, and λ3) *vs*. HAP-BMD of the inserts. HAP, hydroxyapatite; BMD, bone mineral density.